An in-situ IR study on the adsorption of CO2 and H2O on hydrotalcites

Journal of CO_2 Utilization 24 (2018) 228–239

Contents lists available at ScienceDirect

Journal of CO_2 Utilization

journal homepage: www.elsevier.com/locate/jcou

An in-situ IR study on the adsorption of CO_2 and H_2O on hydrotalcites

Kai Coenen, Fausto Gallucci*, Brahim Mezari, Emiel Hensen, Martin van Sint Annaland

Department of Chemical Engineering and Chemistry, Eindhoven University of Technology, P.O. Box 513, Eindhoven, The Netherlands

ARTICLE INFO

Keywords:
In-situ IR
Hydrotalcite
CO_2 Capture
Bidentate carbonate

ABSTRACT

In-situ IR technique was used to study the reversible adsorption of CO_2 and H_2O at elevated temperatures on a potassium-promoted hydrotalcite for its use in sorption-enhanced water-gas shift (SEWGS). It was found that mainly bidentate carbonate species are responsible for the reversible (cyclic) adsorption capacity of the sorbent. The presence of H_2O can enhance the decomposition of bidentate carbonates bond to the stronger basic surface-sites. The basic strength of the involved adsorption sites for bidentate formation appears to be highly heterogeneous. At higher operating temperatures, reversible formation of bulk carbonates seem to participate in the reversible adsorption for CO_2. The presence of H_2O on the sorbent can lead to the formation of bi-carbonate, especially at lower operating temperatures of 300 °C. The transient absorbance of the main absorption bands for carbonate species identified during this study can be used in the development of a detailed description of the reversible adsorption/desorption kinetics reported before using thermogravimetric analyses.

1. Introduction

Hydrotalcites and hydrotalcite-based materials are widely used in several base-catalyzed reactions such as self-condensation and the cross-adol condensation of aldehydes and ketones owing to their basic properties [1]. Hydrotalcite-based materials can also adsorb large quantities of CO_2 in a wide range of temperatures and pressures [2]. Recently, potassium promoted hydrotalcite has been investigated as a potential catalytic adsorbent in the sorption-enhanced water-gas shift (SEWGS) reaction. In SEWGS, CO_2 adsorption to a solid material shifts the equilibrium of the water-gas shift (WGS) reaction, so that a high concentration of hydrogen can be obtained. SEWGS is typically carried out between 350 and 550 °C and allows converting a mixture of CO and water into a nearly pure hydrogen stream [3].

The general formula of hydrotalcite is $M^{2+}_{1-x}M^{3+}_x(OH)_2(A^{n-})_{x/n}\bullet mH_2O$, where M^{2+} is a divalent cation, such as Mg^{2+}, Mn^{2+}, Fe^{2+}, Co^{2+}, Cu^{2+}, Ni^{2+}, Zn^{2+}, or Ca^{2+}, whereas M^{3+} is a trivalent cation, such as Al^{3+}, Cr^{3+}, Mn^{3+}, Fe^{3+}, Co^{3+}, or La^{3+}, and A^{n-} is an anion [4]. The most common stoichiometry for hydrotalcite is the double magnesium-aluminum hydroxide form with the formula $Mg_6Al_2(OH)_{16}CO_3{}^{2-x}\cdot 4\ H_2O$, where the molar ratio of Mg/Al normally varies between 1.7 and 4 [5]. A higher Mg/Al ratio can be beneficial for the adsorption of sour gases because of their higher basicity [6]. On the other hand, mechanical stability issues have been reported for Mg-rich potassium-promoted hydrotalcites due to the formation of $MgCO_3$ at high partial pressures of CO_2 and H_2O [7–9].

The basicity of hydrotalcite-based adsorbents can be further improved by promotion with alkaline anions [9]. It has been frequently reported that K_2CO_3 promotion can increase the sorption capacity of CO_2 [10–12]. Another important aspect is that the initial layered structure of the anionic clay disappears when the material is heated at elevated temperatures. During the heating process the original brucite structure changes to a $Mg(Al)O_x$ mixed metal oxide, releasing CO_2 and H_2O [6,13]. Typical calcination temperatures for hydrotalcites in air after K_2CO_3 promotion are between 673 and 773 K. Higher calcination temperatures can lead to irreversible decomposition of potassium carbonate species, resulting in a lower cyclic working capacity of the adsorbent [11].

Potassium-promoted hydrotalcite sorbents will be exposed to high partial pressures of CO_2 and H_2O (in the order of up to 20 bar of H_2O and CO_2) during their use for SEWGS [14–18]. Therefore, the adsorption and desorption for CO_2 and H_2O adsorption was investigated in the past for a commercially available potassium-promoted hydrotalcite. A complex mechanism was postulated to describe the influence of H_2O on the cyclic working capacity of CO_2 and vice versa [19]. It has been found that at least four different sites are needed to describe the performed thermogravimetric (TGA) and packed-bed reactor (PBR) reactor experiments. However, in which way CO_2 and H_2O are adsorbed by the material and chemically bond to it, is not fully understood yet. Different characterization methods were used in the past to investigate the sorption mechanism of CO_2 on hydrotalcite based materials. X-ray diffraction has been used in various studies to investigate the phases being formed in the material due to the incorporation of CO_2 in its structure [20–23]. However, characterization of the adsorbent is not

* Corresponding author.
E-mail address: F.Gallucci@tue.nl (F. Gallucci).

https://doi.org/10.1016/j.jcou.2018.01.008
Received 25 November 2017; Received in revised form 12 January 2018; Accepted 15 January 2018

Nomenclature

CHT	calcined hydrotalcite
FTIR	Fourier transform infrared spectroscopy
KCHT	potassium promoted calcined hydrotalcite
$K(AL_2O_3)$	potassium promoted alumina
MFC	mass flow controller
PBR	packed bed reactor experiments
SEWGS	sorption-enhanced water-gas shift reaction
TGA	thermogravimentric analysis
WGS	water-gas shift reaction

fully representative, because exposure to ambient will lead to take up of CO_2 and H_2O from the atmosphere. In situ-measurements have shown the formation of Dawsonite ($KAl(CO_3)(OH)_2$) at temperatures below 300 °C for potassium-promoted alumina at high partial pressures of CO_2 and H_2O [24]. For hydrotalcites, the formation of bulk $MgCO_3$ has been reported, which is unwanted [7–9]. X-ray diffraction is not suitable to study the sorption of CO_2 and H_2O as the material is poorly crystalline [25]. FTIR has been frequently used to investigate carbonate species present in hydrotalcites [11,23,26–28]. Du et al. reported that CO_2 reversibly forms unidentate, bidentate and bridged carbonate species, with the formation of bidentate carbonate species being favored at short CO_2 exposure times. The very slow adsorption and desorption properties of CO_2 were assigned to the formation of bulk polydentate carbonates [27]. Bidentate carbonates have been identified as one of the major carbonate species relevant for the CO_2 adsorption mechanism [11], although others have underlined the importance of unidentate carbonate species formed by adsorption of CO_2 on strong basic sites [23]. In order to investigate the desorption of CO_2 and the decomposition of carbonate species, the sorbent is usually exposed to CO_2 at low temperature followed by heating to study desorption. A study where the sample is exposed to CO_2, H_2O and their mixtures as relevant for SEWGS applications and necessary to further investigate the adsorption mechanism is lacking [23,26,29].

In the recent literature, different hydrotalcites and mixed metal oxides were investigated using IR-spectroscopy to determine mainly the different basic strengths of the sites involved in the CO_2 capture mechanism. The basic strength of an adsorption site can depend on the coordination degree of the surface oxygen atoms. The main species formed upon CO_2 adsorption reported are chelating or bridging bidentate carbonates, monodentate carbonates, hydrogen carbonates and CO_2 linear coordinated on M^{n+} sites [26] and are depicted in Fig. 1. The presence of different carbonate species can lead to the need of multiple adsorption sites, if the adsorption and desorption of CO_2 on these types of sorbents is going to be modeled.

It has been reported in the literature, that the free carbonate ion in D_{3h} symmetry has an active IR band at 1415 cm^{-1} (asymmetric ν(CO) vibration). In the adsorbed state the symmetry is lowered and the species formed are usually presented by two ν (CO) bands on both sides of the wavenumber of 1415 cm^{-1}. The distance between both bands on each site of the wavenumber 1415 cm^{-1} is usually reported as $\Delta\nu_3$ splitting [30], which is considered to be a measure of the basic strength of the sites available on the sorbent. A smaller splitting represents stronger basic sites, where unidentate ($\Delta\nu_3$ = 100 cm^{-1}), bidentate ($\Delta\nu_3$ = 300 cm^{-1}) and bridged species ($\Delta\nu_3$ = 400 cm^{-1}) are assigned to be representative carbonate species [30]. In general, different authors in the literature have assigned different carbonate species on potassium-promoted hydrotalcites according to the $\Delta\nu_3$-splitting measured in the experiments. However, it is reported that a low $\Delta\nu_3$-splitting can also indicate the presence of polydentate (very similar to bulk carbonate). It has also been mentioned that a unidentate carbonate would already decompose at relatively low operating temperature (< 150 °C), whereas polydentate is more thermally stable [11,30,31]. Therefore, it is important to consider both the $\Delta\nu_3$-splitting and the operating temperature.

In this work, an in-situ FTIR study was performed on potassium-promoted hydrotalcites under a controlled atmosphere close to SEWGS process conditions relevant for the cyclic exposure to CO_2, H_2O and mixtures of CO_2 and H_2O at elevated temperatures between 300 and 500 °C. This allows the validation of the proposed mechanism of adsorption of CO_2 and H_2O on potassium promoted hydrotalcites.

2. Experimental

The potassium-promoted hydrotalcite sample (KMG30) with a MgO/Al_2O_3 ratio of 0.54 and about 20w% of K_2CO_3 from SASOL, which was already characterized in a previous work [25], was pretreated prior to FTIR measurements at 600 °C in N_2 for two hours to desorb previously adsorbed CO_2 and H_2O from the atmosphere. After the pretreatment around 8 mg of sample was pressed into a self-supporting wafer, which was subsequently placed in the sample holder. After introducing the sample holder in the measuring cell of the FTIR the experimental procedure was started.

In-situ FTIR measurements were performed in a Bruker Vertex 70v FT-IR-spectrometer. The closed measuring cell is used with CaF_2-windows and the cell walls were heated with an external temperature controller to 70 °C to prevent water condensation on the cell-walls. The sample temperature is controlled and can be increased to a maximum temperature of 550 °C.

A manifold was connected to two Brooks mass flow controllers (MFC) for CO_2 and N_2 with a maximum flow rate of 280 Nml/min. The effective pressure between MFC and the cell was set to 0.6 bar (g). Another MFC for N_2 with a maximum flow rate of 200 Nml/min was connected to a saturator. The saturator bottle was filled with H_2O and immersed in a temperature controlled bath, which was kept at a constant temperature of 50 °C. The N_2 gas stream was humidified by passing through the water bottle. All gas lines after the humidifier were traced and heated to above 80 °C to avoid water condensation in the gas lines. Valves V4, V6 and V7 (Fig. 2) were software controlled to prepare

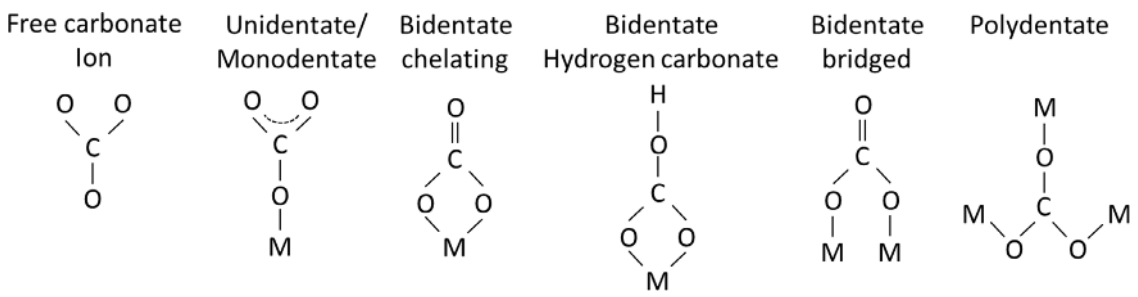

Fig. 1. Different types of carbonate species being formed on hydrotalcite based adsorbents, where the metal can be Al, K or Mg.

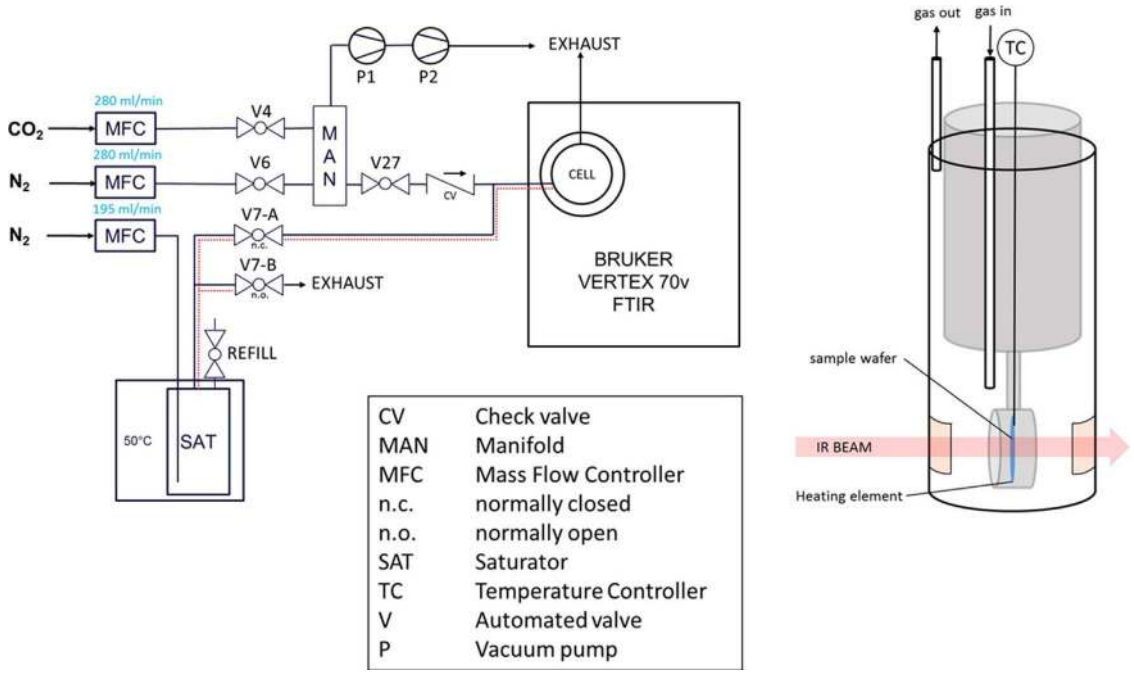

Fig. 2. PFD of automated FTIR-setup and schematic sketch of the measuring cell.

different gas mixtures, which were sent to the measuring cell of the FTIR. Dry gases as N_2 and CO_2 were dosed via the manifold, whereas the humidified gas stream was mixed with the dry gas stream behind the manifold. A check-valve was installed to prevent the humid gas stream entering the manifold. A saturated gas stream of N_2 at 50 °C was constantly produced and either bypassed or sent to the IR-Cell by switching V7-A/V7-B (resulting in a constant saturation of the N_2 stream). Fig. 2 shows a PFD of the setup used for the FTIR measurements.

The reactant gas was injected into the cell close to the sample as indicated in Fig. 2. The flow rates for the different mass flow controllers are chosen in such a way that the maximum possible flow rate is used in order to keep the gas phase transition in the cell as short as possible (to prevent slow mixing and therefore possible effects on the adsorption/desorption of sorbate species). The MFC's were calibrated previously to the experiments using a Definer H-220 to ensure accurate gas dosing under the chosen inlet pressure of the MFC's. The steam content was calculated to be 5%, mixing a dry gas stream (280 ml/min) of CO_2 and N_2 with 195 ml/min of N_2 saturated with water at 50 °C (PH_2O = 0.122 bar). The steam content could not be increased due to limitations of the experimental Setup (avoiding condensation of steam on the IR cell walls and windows). Table 1 shows the carefully designed measurement sequence containing multiple experiments programmed using in-house designed software. Each experiment took 25 min and was divided in 5 sub-segments of 5 min at constant gas flow rate. Every 5 min during a certain experiment, an IR-spectra between 600 and 4000 cm^{-1} with 32 scans was recorded.

In order to be able to follow the changes on the material during in-situ IR, blank measurements have been carried out to measure the absorbance of the gas phase which was used later to correct the recorded spectra with the solid sample. Therefore, three measurements of each gas composition (gas compositions from Table 1, EXP 2, 3, 9 and 21) were carried out. Prior to the blank measurements, the cell was purged with the desired gas composition for 25 min. In order to improve the accuracy, the blank procedure was carried out twice. Blank measurements were conducted for 300, 400 and 500 °C at identical conditions as for the experiments. Five spectra were recorded for each concentration with a 25 min of N_2 purge in between the measurements.

3. Results and discussion

3.1. Background gas-phase spectra

Recorded spectra for three different gas phase compositions, viz. CO_2/N_2, H_2O/N_2 and $CO_2/H_2O/N_2$ as listed in Table 1, are shown in Fig. 3. Typical absorption bands for CO_2 are located at 2300 cm^{-1} corresponding to the asymmetric stretching mode of CO_2 and small peaks in the range 3600–3800 cm^{-1} corresponding to combination bands [32]. For gaseous water two broad bands at around 1600 cm^{-1} and 3600 cm^{-1} are visible. The band at 1600 cm^{-1} is divided into multiple small bands, corresponding to the bending mode of H_2O, where the other branches at 3600 cm^{-1} correspond to the symmetric and antisymmetric stretching mode of H_2O [32]. It was ensured that subtraction of a single gas spectrum (CO_2/N_2 or H_2O/N_2) from a mixed gas spectrum ($CO_2/H_2O/N_2$) would result in the same spectrum measured previously for the remaining gas phase (Fig. 3b). Based on this test it was concluded that indeed a gas phase correction is possible under the selected conditions.

An example for the background gas-phase correction is plotted in Fig. 4, showing the uncorrected spectrum, the spectrum after subtracting the IR spectrum of the same sample before CO_2 adsorption and the corrected spectrum obtained by subtracting the contribution of gaseous CO_2 in order to evaluate the changes at the sorbent surface during adsorption/desorption of CO_2, H_2O.

3.2. Pretreatment of KMG30

To qualify the changes in KMG30 during pretreatment, spectra were recorded prior to pretreatment at room temperature under N_2 atmosphere and after pretreatment (EXP1, Table 1) at an operating temperature of 400 °C. It can be seen (Fig. 5a) that the background absorption of the IR is reduced which can be explained that one background is recorded at 50 °C and the other at 400 °C leading to an absolute change in absorbance. The broad absorption band at 3300 cm^{-1} together with the shoulder at 1650 cm^{-1} disappeared during the heating process to 550 °C during the pretreatment (Step 1, Table 1). The two bands at 1500 cm^{-1} and 1400 cm^{-1} and the band at 1100 cm^{-1} also appear less intense.

Table 1
Experimental procedure used for the in-situ FTIR study, which was carried out at three different operating temperatures (300, 400 and 500 °C). The table shows the procedure for 400 °C.

EXP –	TEMP °C	Time Min	Gas feed –	P N_2 bar	P CO_2 bar	P H_2O bar
1	550	120	N_2	1.00		
2	400	25	N_2	1.00		
3	400	25	N_2/CO_2	0.50	0.50	
4	400	25	N2	1.00		
5	400	25	N_2/CO_2	0.50	0.50	
6	400	25	N_2	1.00		
7	400	25	N_2/CO_2	0.50	0.50	
8	400	25	N_2	1.00		
9	400	25	N_2/H_2O	0.95		0.05
10	400	25	N_2	1.00		
11	400	25	N_2/H_2O	0.95		0.05
12	400	25	N_2	1.00		
13	400	25	N_2/CO_2	0.50	0.50	
14	400	25	N_2	1.00		
15	400	25	N_2/H_2O	0.95		0.05
16	400	25	N_2	1.00		
17	400	25	N_2/CO_2	0.50	0.50	
18	400	25	N_2	1.00		
19	400	25	N_2/H_2O	0.95		0.05
20	400	25	N_2	1.00		
21	400	25	CO_2/H_2O	0.45	0.50	0.05
22	400	25	N_2	1.00		
23	400	25	N_2/H_2O	0.95		0.05
24	400	25	N_2	1.00		
25	400	25	CO_2/H_2O	0.45	0.50	0.05
26	400	25	N_2	1.00		
27	400	25	N_2/H_2O	0.95		0.05
28	400	25	CO_2/H_2O	0.45	0.50	0.05
29	400	25	N_2/H_2O	0.95		0.05
30	400	25	CO_2/H_2O	0.45	0.50	0.05
31	400	25	N_2/H_2O	0.95		0.05
32	400	25	N_2	1.00		
33	400	25	CO_2/H_2O	0.45	0.50	0.05
34	400	25	N_2/CO_2	0.50	0.50	
35	400	25	CO_2/H_2O	0.45	0.50	0.05
36	400	25	N_2/CO_2	1.00		
37	400	25	N_2	1.00		

The disappearance of the broad peak around 3300 cm^{-1} is caused by desorption of H_2O from the sample. Bands at 3400 cm^{-1} are typically for symmetric O—H stretching and at 3506 cm^{-1} for asymmetric O—H stretching. Various carbonate species such as free carbonate anion (hydroxyl carbonate) and unidentate and bidentate carbonate species decompose resulting in reduced absorbance in the 1400–1500 cm^{-1} range and at 1100 cm^{-1} [29,33]. These changes are consistent with the reported release of H_2O and CO_2 during pretreatment by TGA and TGA-MS [25]. Despite the release of CO_2, the IR spectrum shows that some carbonate species persist after the pretreatment procedure. Based on the low $\Delta\nu_3$-splitting (150 cm^{-1}) for the two remaining absorption bands at 1535 and 1380 cm^{-1} and the high thermal stability of the remaining carbonates, we conclude that these are strongly bound bulk or polydentate carbonate species [11,30,31,33]. The small remaining band at 3500 cm^{-1} (Fig. 5b) reveals that still small number of OH-groups are present on the sorbent surface after the pretreatment.

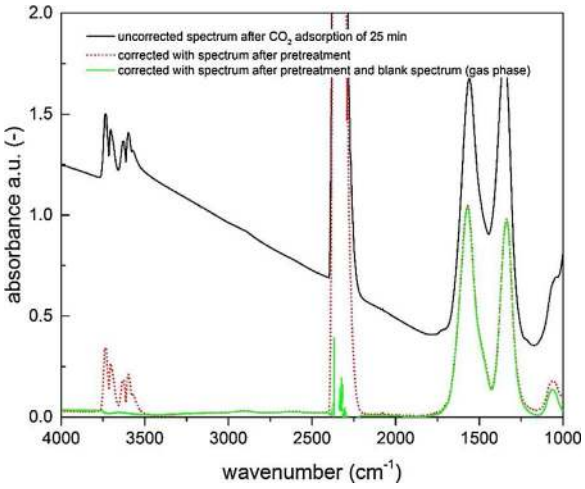

Fig. 4. Recorded spectra after CO_2 adsorption and correction of spectra with blank.

3.3. Adsorption of CO_2 and desorption with N_2

Fig. 6a shows the changes in the IR spectrum upon exposure of the pretreated sample to CO_2 at 400 °C between 1000 and 1900 cm^{-1}, since only visible changes in the IR-spectra were detected in this region. Exposure to CO_2 increases the intensity of the bands at 1570, 1340 and 1060 cm^{-1}. The most prominent increase is observed in the first 5 min followed by a slower increase during the total exposure of 20 min. These kinetics are in keeping with the CO_2 uptake observed in TGA-MS studies [19].

Upon exposure to N_2 for 25 min (Fig. 6b) the absorption bands at 1570 cm^{-1}, 1340 cm^{-1} and 1060 cm^{-1} decrease again. Not all CO_2 adsorbed in step 3 can be desorbed under these conditions. The decreased $\Delta\nu_3$-splitting can be attributed to the heterogeneity in CO_2 binding. That is to say, during CO_2 desorption first relatively weakly adsorbed CO_2 is released followed by stronger bound CO_2. Based on the $\Delta\nu_3$-splitting of 235 cm^{-1} (after CO_2 adsorption) and 220 cm^{-1} (after desorption of CO_2 with N_2), we can conclude that mainly bidentate carbonate species are formed during the adsorption of CO_2 on KMG30, as unidentate carbonate species are usually not stable at 400 °C [31].

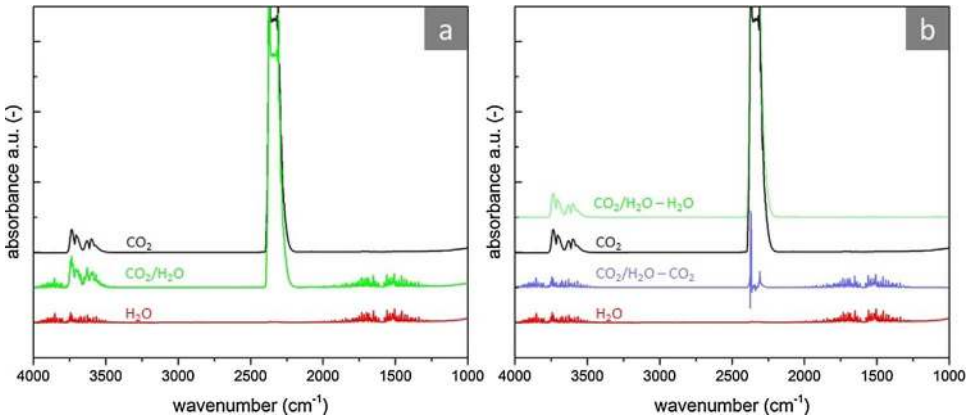

Fig. 3. IR gas-phase spectra. Baseline for the spectra is increased to make the different spectra visible a) Measured gas phases spectra of different gases b) measured gas phase spectra for CO_2 and H_2O and spectra of mixture of CO_2/H_2O which was corrected with pure gas spectra for H_2O (green) which should correspond to the gas spectra of CO_2 and once with CO_2 (violet) which should correspond to the gas spectra of H_2O. (For interpretation of the references to colour in this figure legend, the reader is referred to the web version of this article.).

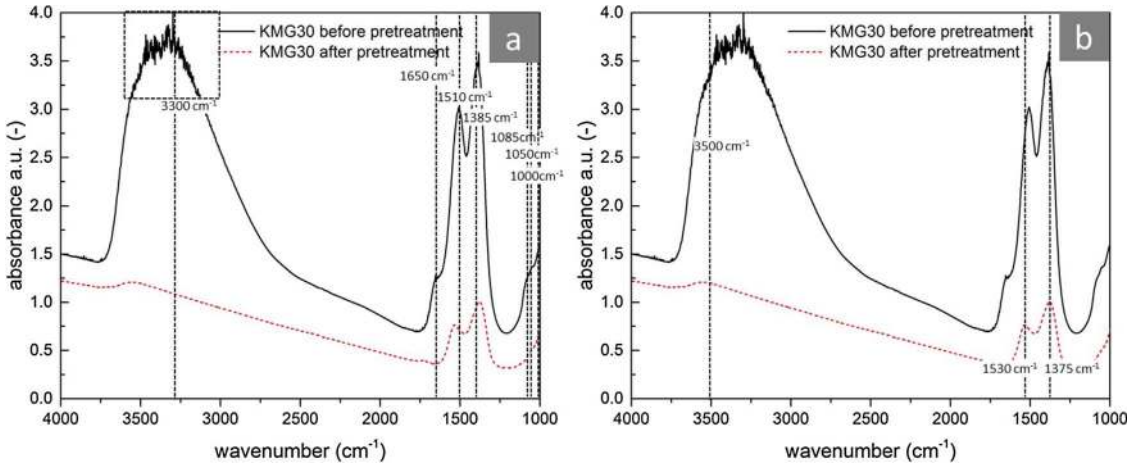

Fig. 5. Spectra recorded before and after the pretreatment Assignments of absorption bands before (a) and after (b) pretreatment of KMG30.

According to the literature, most probably chelating bidentate or bridged carbonate structures are present under these conditions ($\Delta\nu_3 < 250\,cm^{-1}$) [11,30,31]. The band CO_2 at $1060\,cm^{-1}$ becomes slightly IR-active upon CO_2 adsorption for various carbonate species as unidentate and bidentate [23,30].

Comparing the spectra after adsorption of CO_2 after the second adsorption cycle with the first adsorption cycle (Fig. 6c, EXP5), some differences can be seen. The total absorbance is increased compared to the first cycle. It is known that a steady state between adsorption and desorption is established after a certain number of cycles [25]. Therefore, the increased absorbance is attributed to a higher loading of CO_2 in the form of carbonate species. Again, an increase in $\Delta\nu_3$-splitting ($235\,cm^{-1}$) can be obtained from Fig. 7 indicating the reversible formation of weaker bond bidentate.

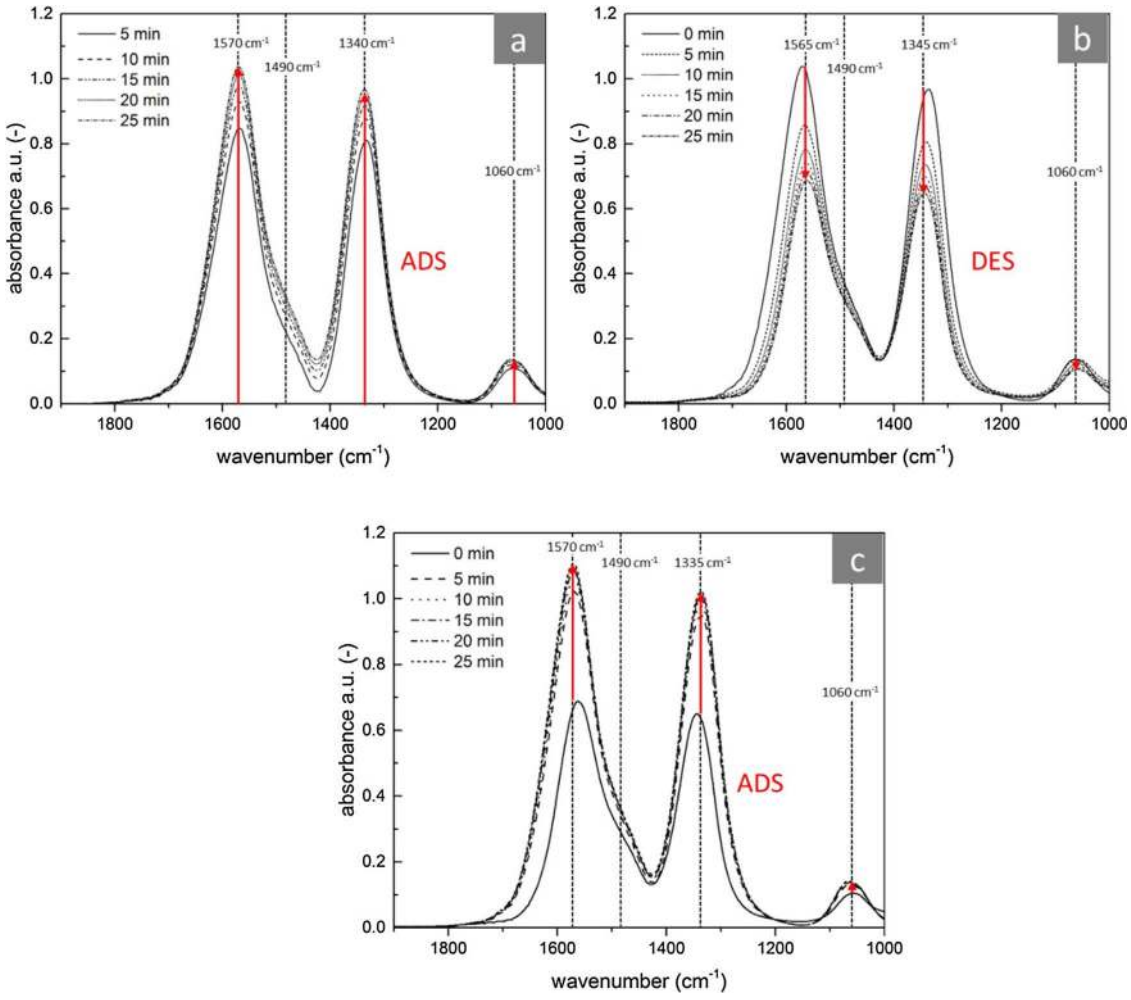

Fig. 6. a) Spectra recorded at different times during the first adsorption of CO_2 at 400 °C (EXP3) b) Spectra recorded at different times during desorption of CO_2 with N_2 at 400 °C (EXP4) c) Spectra recorded at different times during the second adsorption cycle of CO_2 at 400 °C (EXP5).

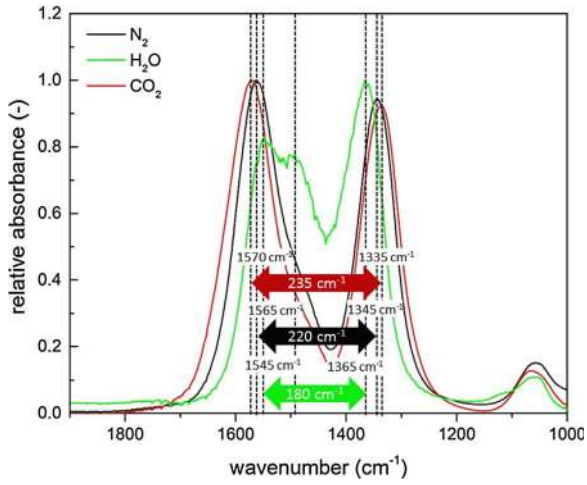

Fig. 7. Normalized spectra to the maximum absorbance after exposure to CO_2, H_2O and N_2 to visualize the change in $\Delta\nu_3$-splitting upon exposure to different gases at 400 °C.

3.4. Adsorption of CO_2 and desorption with H_2O

The IR spectra during adsorption of H_2O during experiment 9 is plotted in Fig. 8a, together with the last recorded spectrum of experiment 8 as reference (time zero). A broad absorption band at 3500 cm^{-1} and a small increase in the absorption band at 1430 cm^{-1} is visible in this step (Step 9, feed of N_2 and H_2O). The broad band at 3500 cm^{-1} can be assigned to the adsorption of H_2O (symmetric and asymmetric O—H stretching) on the sorbent.

The absorbance of the absorption bands at 1565, 1365 and 1060 cm^{-1} strongly decreases, which can be attributed to the decomposition of bidentate carbonate upon exposure to H_2O and N_2. The maximum of the absorption bands are shifted (1565 → 1550 cm^{-1}, 1350 →1365 cm^{-1}) during this experiment, similar to the desorption step of CO_2 with N_2. The further decrease in $\Delta\nu_3$-splitting (indicated by the shift in the maximum of the absorption bands) to 185 cm^{-1} (Fig. 7) indicates that the CO_2 desorbed from the sorbent during this step was indeed strongly bound, confirming our hypothesis, that very heterogeneous sites are present on the sorbent for CO_2 adsorption. It seems that adsorbed H_2O can reduce the amount of available strong basic adsorption sites for CO_2 and therefore initiating the decomposition of stronger bond carbonate species. This explains the decrease in desorption rate because the remaining carbonate species on the material were formed on more basic sites (for both desorption with N_2 and desorption with H_2O). Again the major decomposition of carbonate takes place during the first 5 min as reported earlier using TGA [19]. In contrast to the desorption with N_2 where both absorption bands were decreasing in the same way, in case of H_2O being present, the band at 1550 cm^{-1} has decreased significantly more and a small shoulder at 1490 cm^{-1} becomes visible. The shape of the remaining bands (similar to the remaining carbonates after the pretreatment) indicates that some bulk carbonate or polydentate and additionally some bicarbonates (band at 1490 cm^{-1}) are formed.

If the material is exposed to N_2 during experiment 10 (Fig. 8b), only a small decrease of the absorption band at 3500 cm^{-1} can be observed, whereas the other bands seem to remain nearly unchanged. If CO_2 is fed again to the material, the bands at 3500 and 1430 cm^{-1} are decreasing, whereas the bands at 1550, 1365 and 1060 cm^{-1} are increasing

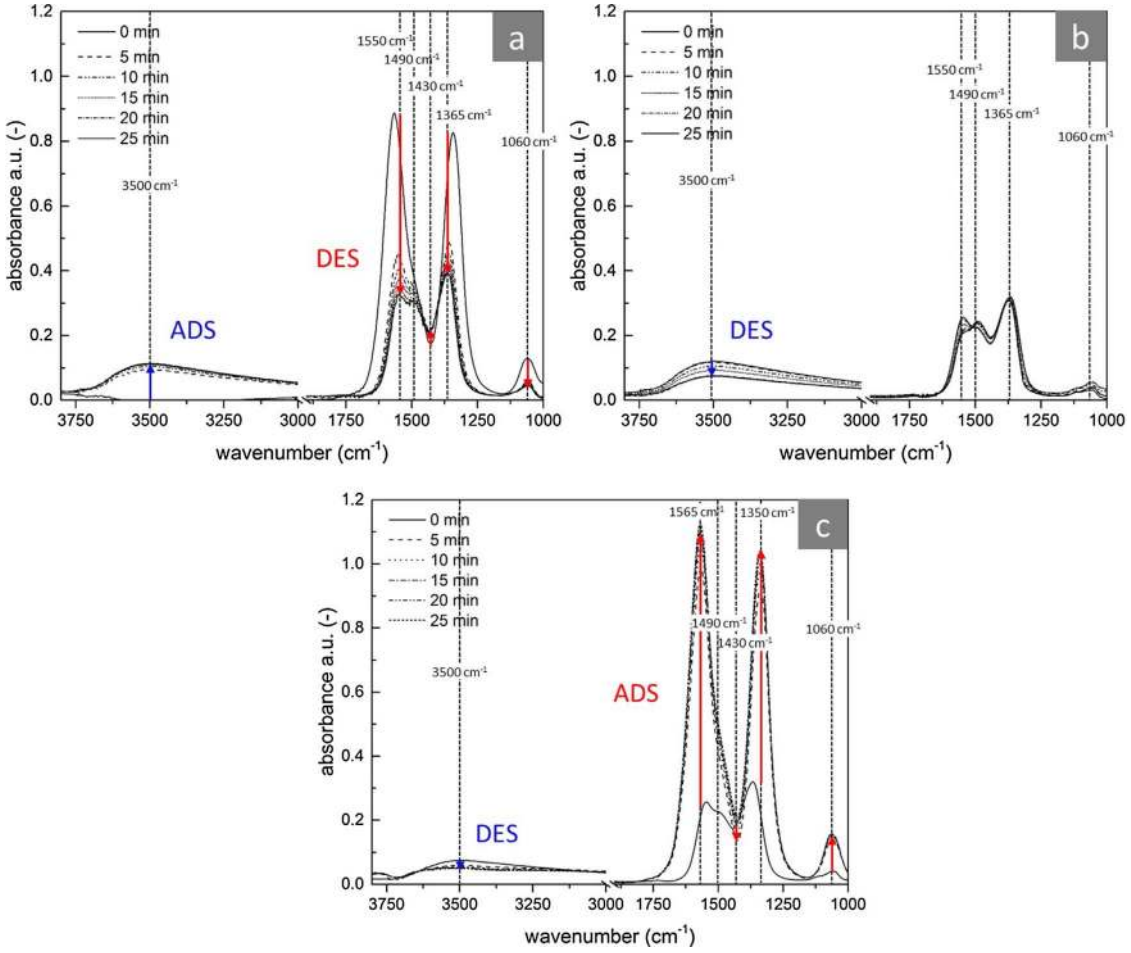

Fig. 8. a) Adsorption of H_2O at 400 °C (EXP9) b) Desorption of H_2O at 400 °C with N_2 (EXP10) c) Adsorption of CO_2 at 400 °C after desorption with H_2O and N_2 (EXP13).

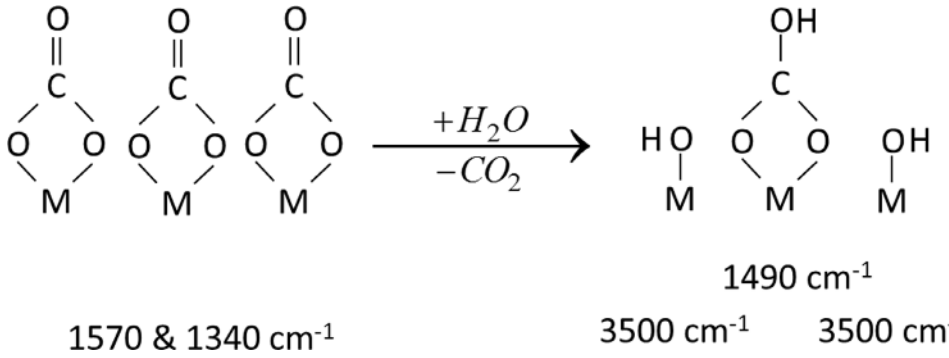

Fig. 9. Partial conversion of bidentate carbonate to hydrogen carbonate upon exposure to H_2O on the surface of the adsorbent.

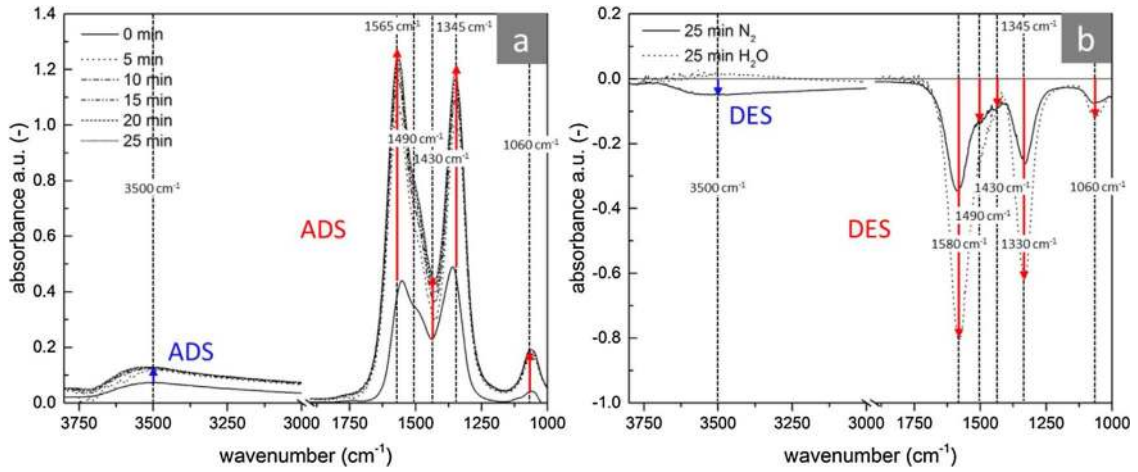

Fig. 10. a) Adsorption of CO_2/H_2O at 400 °C (EXP21) b) Change in absorbance during desorption of CO_2 with either N_2 or H_2O after adsorption of CO_2/H_2O at 400 °C (N_2: EXP19, H_2O: EXP26).

(Fig. 8c). These results show that during the CO_2 adsorption additional H_2O is desorbed. It was already reported, that adsorption of CO_2 leads to additional desorption of H_2O, which is now also confirmed by these results using in-situ IR [19]. Both, the very fast adsorption of H_2O postulated in the previous publication and the rapid replacement is confirmed. It becomes evident, that probably only one carbonate species is responsible for the adsorption mechanism at high temperature. However, the strength of the interaction between CO_2 in adsorbed state and the basic oxygen atoms seem to be different and not homogeneous.

The increase of the absorption band at 1490 cm^{-1} is exceptional since the other absorption bands in this region show a decrease in absorbance as expected. A possible explanation could be that strongly bond bidentate carbonate which could not be desorbed, is converted into bi-carbonate (hydrogen carbonate) due to the presence of H_2O on the surface of the sorbent like illustrated in Fig. 9. However, a clear identification is difficult because the expected presence of the absorption bands around 1650 and 1220 cm^{-1} (typical for hydrogen carbonate) was not observed from the recorded spectra.

During the adsorption of CO_2 in experiment 13, the decrease in the broad band at 3500 cm^{-1} indicates a further desorption of H_2O. It has

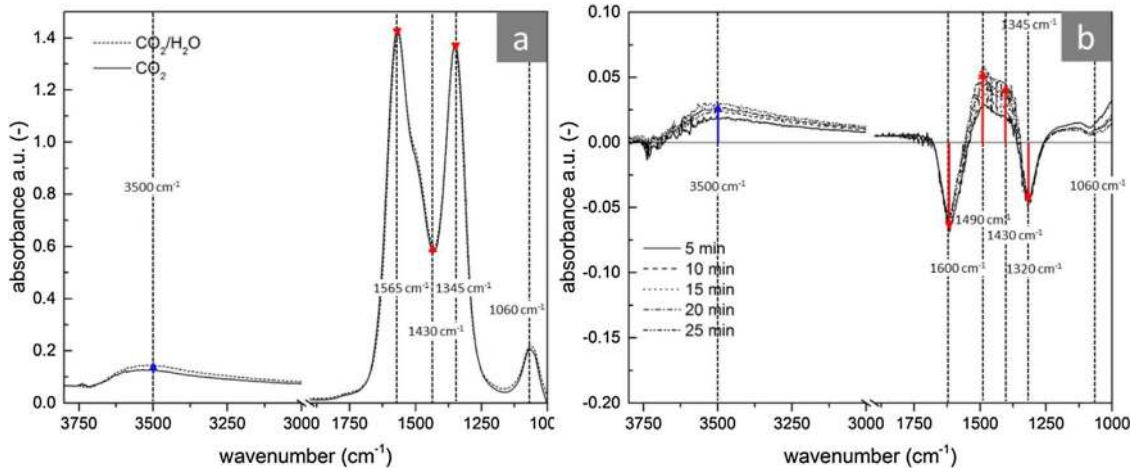

Fig. 11. a) Corrected spectra for Experiments 34 (CO_2) and 35 (CO_2/H_2O) and at 400 °C b) Net change in absorbance between experiment 34 and 35 to elucidate the replacement effect on KMG30.

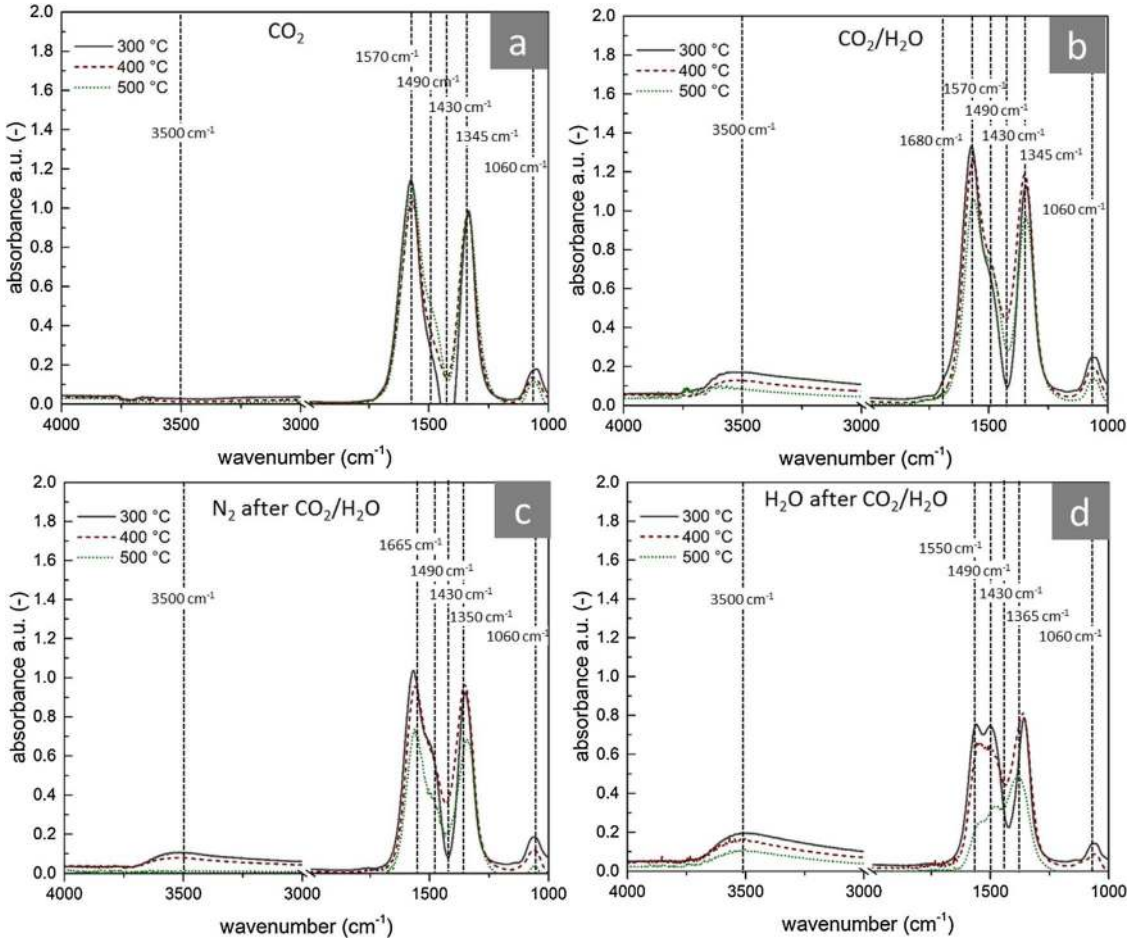

Fig. 12. a) Spectra recorded after CO_2 adsorption (EXP2) b) Spectra recorded after CO_2/H_2O (EXP19) c) Spectra recorded after N_2 (EXP20) d) Spectra recorded after H_2O (EXP27).

been found in earlier studies that indeed CO_2 is required to desorb additional amount of H_2O, which cannot be removed with N_2. The band at 1430 cm^{-1} decreases in the same way as it increased during the adsorption of H_2O in experiment 9. In the literature this single absorption band is assigned to the formation of bulk carbonates [11]. This would imply that H_2O can lead to the formation of reversible bulk carbonate. The bands at 1550, 1365 and 1060 cm^{-1} are reaching the same net absorbance as during experiment 5, indicating that the same carbonate species are formed as prior to the exposure of the material to H_2O.

3.5. Adsorption of CO_2/H_2O and desorption with H_2O and N_2

Co-adsorption of CO_2 and H_2O was studied with experiment 21. Fig. 10a shows the changes of the absorption bands during the adsorption of CO_2 and H_2O. Similar to the experiments where only CO_2 was used, the bands at 1565, 1345 and 1060 cm^{-1} are increased significantly. Again, the broad absorption band at 3500 cm^{-1} is increasing upon adsorption of H_2O. However, differently to the previous experiment, a strong increase of the band at 1430 cm^{-1} can be observed during this experiment. It was reported that indeed upon CO_2/H_2O exposure the adsorbent showed a significant weight increase during TGA experiments, which can be explained now by the formation of bulk carbonates [19].

In Fig. 10b the changes in the recorded IR-spectra are plotted when either N_2 or H_2O is used after the adsorption of CO_2/H_2O. Note that the plotted absorbance is the net change compared to the spectra recorded previously after CO_2/H_2O adsorption. The decrease in the absorption bands between 1600 and 1000 cm^{-1} is significantly higher if the sorbent is exposed to H_2O. The broad absorption band at 3500 cm^{-1} remains unchanged during the experiment with H_2O, whereas a decrease can be obtained if N_2 is used instead. The difference in absorbance decrease of the bands at 1580, 1490, 1330 and 1060 cm^{-1} show that the desorption of CO_2 is improved if H_2O is used during the desorption step. The absorption band at 1430 cm^{-1} show a smaller intensity decrease compared to the experiment where N_2 was used. This can be explained with the reversible formation of bulk carbonates. Surface OH groups can only be desorbed if the partial pressure of H_2O is lowered (feed of N_2).

3.6. Competitive adsorption effects

To further study the effect of H_2O inducing desorption of CO_2 and vice versa during experiments 33–36 the partial pressure of CO_2 was kept constant while changing the partial pressure of H_2O. It was decided to study the replacement effect of CO_2/H_2O after dry CO_2, since it is known from recorded gas phase spectra that small amounts of H_2O seem to be present in the cell still after 5 min, which therefore cannot be used if we want to study the immediate effect on the sorbent. It can be seen from Fig. 11a that indeed only small changes are visible between the two spectra. The absorption bands at 3500 and 1430 cm^{-1} are increased slightly, whereas the absorption bands at 1565 and 1345 cm^{-1} are decreased slightly if a CO_2/H_2O gas stream is fed to the cell. The net change in absorbance (Fig. 11b) provides a better view to the changes on the material. It can be seen that the bands at 3500 and 1490 cm^{-1} are increasing and both bands at 1600 and 1320 cm^{-1} decreasing. Decrease in absorbance seems to be time independent (no change after 5 min) where the increase in the band at 1490 cm^{-1} seems to be slower

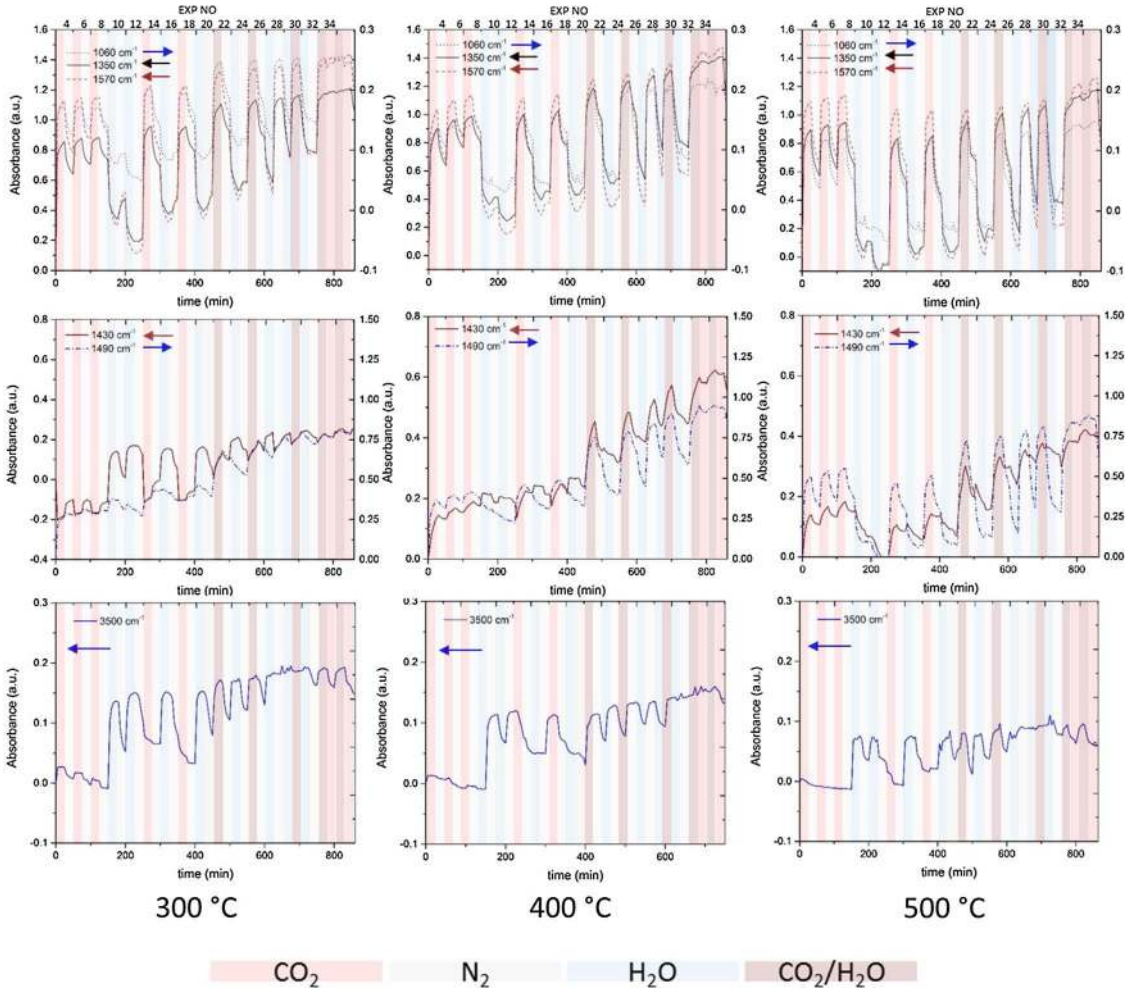

Fig. 13. Absorbance evolution of different wavelengths at different temperatures as function of time (and experiment number). The distinct colors indicate a change in the gas phase composition during a specific experiment. Arrows are indicating the legend for a certain monitored wavenumber.

and not finished after 25 min.

One has to notice that the partial pressure of H_2O used during this experiment is quite low and therefore the replacement effect is expected to be small in this case due to the relative high partial pressure of CO_2 compared to H_2O. Taking into account the $\Delta\nu 3$-splitting of the decreasing absorption bands being 280 cm^{-1}, bidentate carbonate is desorbed from the sorbent during this step. This would explain the instantaneous replacement and fast kinetics for this adsorption site which we have reported earlier [19]. The increased absorption of the band at 1490 cm^{-1} again can be explained by the formation of hydrogen carbonate due to the presence of H_2O and CO_2 on the sorbent. It was observed that indeed if the feed gas was changed to dry CO_2 the observations described here are reversible.

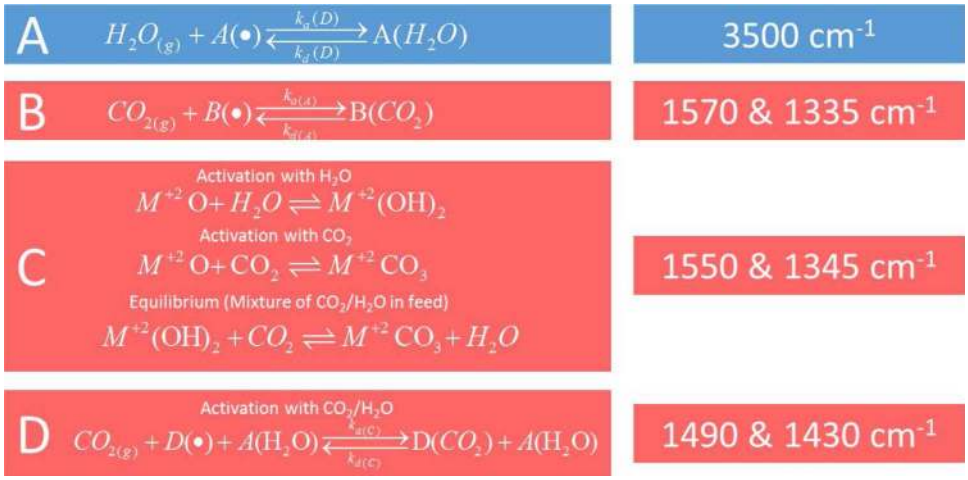

Fig. 14. Proposed mechanism for H_2O and CO_2 adsorption on KMG30 and IR bands assigned to different adsorption based on the experimental results.

3.7. Influence of temperature on carbonate species

Experiments were conducted according to Table 1 at 300 and 500 °C and compared to the results obtained for 400 °C in order to study the influence of operating temperature on the reversible formation of carbonates. Fig. 12(a–d) show the recorded spectra at different operating temperature for four different feed gas compositions.

Fig. 12a shows the spectra recorded during experiment 2 using a dry CO_2 gas stream. The net change in absorbance of the bands 1570, 1345 and 1060 cm^{-1} are very similar, with a somewhat higher absorbance of the band at 1570 cm^{-1} at lower temperature. The absorbance for the bands at 1490 and 1430 cm^{-1} is increased at higher operating temperature. The small differences between the spectra indicate that the amount of CO_2 adsorbed at different operating temperature is the same, which has been reported using TGA previously [25]. The difference of the bands at 1430 and 1490 cm^{-1}, however, show that the carbonate species formed do not have to be the same. At higher operating temperature, more bulk carbonate seem to be formed which could be explained by an increased diffusion of carbonate species from the surface to the bulk of the sorbent. The higher absorbance for the band at 1570 cm^{-1} for lower temperatures indicates that the amount of weaker bond CO_2 is increased.

After CO_2/H_2O adsorption (Fig. 12b, EXP19) most of the absorption bands are decreasing with an increasing operating temperature. This can be expected, since it is known that at lower temperatures a higher irreversible adsorption of CO_2 is taking place, caused by slower desorption kinetics [19]. The reduced absorbance for the band at 3500 cm^{-1} indicates a lower amount of H_2O being adsorbed at higher temperature. However, it would be expected that at higher temperature the formation of bulk carbonate (1490 cm^{-1}) would be enhanced like in the experiment with a dry feed gas. It seems that the presence of adsorbed H_2O somehow can enhance the formation of bulk carbonates. At 300 °C a small shoulder is visible at 1650 cm^{-1} indicating the formation of some bicarbonate.

During a desorption step with either N_2 or H_2O in both cases a larger decrease in the absorbance is obtained at higher temperature (Fig. 12c and d). Due to in general increased desorption kinetics at higher operating temperatures, the results are supporting previous measurements, that indeed the CO_2 loading on the sorbent is decreased by increasing the operating temperature. This is confirmed by the lower absorption of the bands at 1680–1060 cm^{-1}.

If H_2O is used for the regeneration of adsorbed CO_2 (Fig. 12d), the absorbance of the different bands is further decreased compared to the regeneration with N_2. It can be obtained that the absorption of all bands is again decreased for a higher temperature indicating that more of the previously adsorbed CO_2 can be desorbed. Due to the strong decrease of the band at 1550 cm^{-1} (which is lower at higher temperature) the band at 1490 cm^{-1} becomes more visible. Together with the fact that the $\Delta\nu_3$-splitting seems to be reduced at higher temperatures we can conclude that at higher temperatures even stronger bond carbonate species can be desorbed. The desorption of CO_2 (by feeding N_2) at higher operating temperature can be increased in the same way as using H_2O as a feed at lower temperature. A combination of both (high operating temperature and H_2O present during desorption of CO_2) is therefore the reason for a higher cyclic working capacity obtained in earlier TGA measurements. The clearly visible band at 1490 cm^{-1} (Fig. 12d) at lower temperature indicates that some bicarbonate is remaining. Since also H_2O cannot be desorbed at lower operating temperature it can be expected that this carbonate species remains. This hypothesis is confirmed in the literature where K-dawsonite ($KAl(CO_3)(OH)_2$) formation has been reported for this sorbent which has been detected at lower operating temperature (and could be one possible species formed on the sorbent). If the operating temperature is increased this phase seems to disappear [8,20]. The complete disappearance of the band at 1060 cm^{-1} at 500 °C indicates that the remaining carbonates are probably some bicarbonates and bulk carbonates (polydentate) with a

Table 2
Band positions and carbonate species reported in the literature for hydrotalcites and similar materials (CHT = calcined hydrotalcite).

Material	free carbonate	unidentate carbonate		bidentate carbonate		bridged carbonate		polydentate		bicarbonates		Reference
		ν_{as}	ν_s	ν_{as}	ν_s	ν_{as}	ν_s	ν_{as}	ν_s	ν_{as}	ν_s	
$Al_2O_3(OH)$	1450			1704	1265	1756	1204					[33]
MgO				1686	1365			1659	1304	1630	1452	1217
										1600	1448	1200
CHT		1591–1574	1386–1365	1658–1650	1420–1400					1655	1405	1220
MgO	1410	1550–1520	1410–1390	1670–1630	1320–1275							[31]
α-Al_2O_3		1610–1570	1385–1350	1710	1310	1810–1730	1310			1655	1440	1227
γ-Al_2O_3		1530	1370	1730–1660	1270–1230	1900–1750	1180			1659–1650	1490–1440	1236–1225
CHT		1560-1510	1400-1360	1630-1610	1340-1320					1650	1480	1220
MgO/Al_2O_3	1415											1230
$\Delta\nu_3$		> 80		> 250		< 250						[4]
$\Delta\nu_3$		100		300		400						[36]
CHT		1575–1590	1355–1385			1645–1655	1325	1730–1755	1300–1325			
$\Delta\nu_3$		70 - 125										[23]
		1500–1530	1385–1435									
$\Delta\nu_3$		190–235										
K(Al2O3)				1560	1362					1655	1520	1410
$\Delta\nu_3$				198								[11]
CHT	1430			1560	1370							
$\Delta\nu_3$				190								
CHT	1430			1570–1540	1365–1335							This work
$\Delta\nu_3$				185–235								

high thermal stability.

3.8. Transient behavior of carbonate formation

To show the relative absorbance of the different adsorption bands, changing during the experiments as a function of time, the relative net absorbance of different characteristic wavenumbers is plotted in Fig. 13. The first two rows show the absorption bands which has been assigned to carbonates. On the third row the absorbance of the band at 3500 cm^{-1} is plotted, which has been assigned to H_2O adsorbed by the adsorbent. As indicated in the legend, the different background color indicates which mixture of gases was present in the cell.

It can be observed that the net change in absorbance is higher for higher temperatures for the bands 1060, 1350 and 1570 cm^{-1}, confirming that the amount of CO_2 being exchanged is increased in at higher temperatures. In general, a larger irreversible formation of carbonate species due to the slower desorption kinetics of certain absorption bands (e.g. 1060 and 1570 cm^{-1}) can be obtained from these figures, which are supporting results earlier obtained by TGA measurements [19]. It is remarkable how the measured weight change by TGA experiments is directly comparable to the absorbance of certain bands. This shows how in-situ IR can be extremely useful to follow CO_2 adsorption on hydrotalcite-based sorbents and how H_2O influences CO_2 adsorption. Even if the partial pressure of CO_2 is kept constant it can be seen that the absorbance of certain absorption bands is higher with dry CO_2 as a feed gas compared to a wet gas stream which is more distinct at higher temperatures (Fig. 13 first row, 1570 cm^{-1}). The net absorbance change of the carbonate species in this region seems to match the measured weight change as function of time. In general, it can be derived that both the initial adsorption/desorption are quite fast, where the change in absorbance (e.g. adsorption/desorption of CO_2) appears to be slower. These results show that the amount of the remaining carbonate species could be further decreased by increasing the desorption time which has been described in the past using TGA measurements [25].

The net absorption of the band at 3500 cm^{-1} is increased at lower temperature. We have already reported that the cyclic working capacity for H_2O is significantly increased at lower temperatures due to the higher adsorption capacity for H_2O of the sorbent at lower temperatures. It has been reported in the literature using coupled TGA and in-situ IR, that the absorbance of the region between 3000 and 3500 cm^{-1} increases in the same way as the adsorption of water [34,35]. These observations are supported by our measurements which show the same behavior comparing the net change in absorbance to TGA measurements conducted at different operating temperatures.

Comparing the obtained results during this study to a previous study using thermogravimetric analysis and packed bed reactor experiments [19] to determine the cyclic working capacity of CO_2 and H_2O on KMG30, the proposed mechanism can be confirmed. The absorption bands at 1060, 1335 and 1570 cm^{-1} can be assigned to the two sites necessary to describe the adsorption of CO_2 and H_2O. Considering the $\Delta\nu_3$-splitting, it seems that a very heterogeneous site strength distribution of mostly bidentate carbonate species is responsible for the adsorption of CO_2. The regeneration with H_2O can enable the decomposition of stronger bond bidentate carbonate species. This conclusion is based on the lower $\Delta\nu_3$-splitting of the remaining carbonates and can be attributed to site C. With this the two sites B (1570 & 1335 cm^{-1}) and C (1550 & 1345 cm^{-1}) for CO_2 can be described (Fig. 14).

The irreversible adsorption and activation of an additional site by feeding CO_2 and H_2O to the adsorbent is confirmed by the significant changes of the bands at 1430 and 1490 cm^{-1} and therefore to the formation of bulk carbonate and some bicarbonates which can be attributed to the proposed site D for CO_2. A longer desorption time can reduce the amount of site D required to describe the adsorption capacities on the sorbent due to the slow continuous desorption of the stronger bond carbonate species which was proved recently with TGA experiments.

The adsorption of H_2O indicated by the broad adsorption band at 3500 cm^{-1} can be assigned to the proposed site A.

If we compare the absorption bands detected during this study with results obtained and reported in the literature (Table 2) one can conclude that the results are comparable to some of the results already published in the literature. The band at 1490 cm^{-1} has been identified as a hydrogen carbonate (which usually comes together with two bands at 1220 and 1650 cm^{-1} [4]) which can be present due to the formation of K-dawsonite ($KAl(CO_3)(OH)_2$). This has been reported in the literature for the same adsorbent [11,24]. The formation of bidentate carbonate (1590–1355 cm^{-1} and 1090 cm^{-1}) was reported by various authors for similar types of sorbents, confirming our findings, that indeed this type of carbonate is mainly responsible for the CO_2 sorption capacity on this sorbent. Reversible bulk carbonate formation and the formation of bicarbonate were reported at different experimental conditions. However, no studies have been found using in-situ IR under realistic operating conditions using both CO_2 and H_2O as sorbate species.

4. Conclusions

In-situ IR has been used to elucidate the adsorption of CO_2 and H_2O on a hydrotalcite based adsorbent (KMG30). It has been shown that mostly a heterogeneous distribution of thermally stable bidentate carbonate sites with different basic strength are determining the adsorption and desorption kinetics of CO_2 on the sorbent. The presence of H_2O seem to enable the decomposition of even stronger bound bidentate carbonate sites leading to an increase in the cyclic working capacity, as reported by various authors in the literature, confirming also results published recently. It has been shown that the desorption kinetics are determining the cyclic CO_2 working capacity of the material due to the increased bond strength of remaining carbonate species on the sorbent, leading to a decrease in the desorption rate if the CO_2 loading on the material decreases.

In addition, it could be confirmed that feeding CO_2 to a hydroxylated sorbent (feeding CO_2/H_2O) seems to initiate the formation of some bicarbonates. K-dawsonite formation can be one possible compound formed on the sorbent. Both a higher operating temperature and the presence of H_2O seem to enhance the formation of some bulk carbonates.

At constant partial pressures of CO_2 additional CO_2 can be adsorbed if the partial pressure of water is lowered. In the same way we could obtain an additional desorption of H_2O if the sorbent was exposed to a dry CO_2 stream. These observations are important and supportive to results published earlier where TGA and packed-bed breakthrough experiments have been used to determine the cyclic working capacity for CO_2 and H_2O of the adsorbent.

Finally, it could be confirmed that the increase in the cyclic working capacity at higher operating temperature is due to the decomposition of stronger carbonate species and therefore leading to a lower CO_2 loading of the sorbent at the end of a desorption step.

These results support the development of a model for the adsorption and desorption kinetics of CO_2 and H_2O mixtures on hydrotalcites for the design and optimization of SEWGS processes.

Acknowledgements

The research leading to these results has received support through the ADEM innovation lab program, project number TUE-P05.

References

[1] S. Abelló, F. Medina, D. Tichit, J. Pérez-Ramírez, X. Rodríguez, J.E.E. Sueiras, P. Salagre, Y. Cesteros, Study of alkaline-doping agents on the performance of reconstructed Mg–Al hydrotalcites in aldol condensations, Appl. Catal. A Gen. 281

(1–2) (2005) 191–198 Mar..
[2] Z. Yong, V. Mata, A.E. Rodrigues, Adsorption of carbon dioxide at high temperature - a review, Sep. Purif. Technol. 26 (2–3) (2002) 195–205.
[3] E.R. van Selow, P.D. Cobden, Ha.J. van Dijk, S. Walspurger, Pa. Verbraeken, D. Jansen, Qualification of the ALKASORB sorbent for the sorption-enhanced water-gas shift process, Energy Procedia 37 (2013) 180–189.
[4] J.I. Di Cosimo, V.K. Díez, M. Xu, E. Iglesia, C.R. Apesteguía, Structure and surface and catalytic properties of Mg-Al basic oxides, J. Catal. 178 (No. 2) (1998) 499–510.
[5] W.T. Reichle, Catalytic reactions by thermally activated, synthetic, anionic clay minerals, J. Catal. 557 (No. 2) (1985) 547–557. Aug..
[6] D.P. Debecker, E.M. Gaigneaux, G. Busca, Exploring, tuning, and exploiting the basicity of hydrotalcites for applications in heterogeneous catalysis, Chemistry 15 (No. 16) (2009) 3920–3935 Jan..
[7] E.R. van Selow, P.D. Cobden, R.W. van den Brink, J.R. Hufton, A. Wright, Performance of sorption-enhanced water-gas shift as a pre-combustion CO2 capture technology, Energy Procedia 1 (no. 1) (2009) 689–696 Feb..
[8] E.R. Van Selow, P.D. Cobden, A.D. Wright, R.W. Van Den Brink, D. Jansen, Improved sorbent for the sorption-enhanced water-gas shift process, Energy Procedia 4 (2011) 1090–1095 Jan..
[9] S. Walspurger, P.D. Cobden, O.V. Safonova, Y. Wu, E.J. Anthony, High CO(2) storage capacity in alkali-promoted hydrotalcite-based material: in situ detection of reversible formation of magnesium carbonate, Chemistry 16 (No. 42) (2010) 12694–12700 Nov..
[10] N.N.A.H. Meis, J.H. Bitter, K.P. De Jong, On the influence and role of alkali metals on supported and unsupported activated hydrotalcites for CO2 sorption, Ind. Eng. Chem. Res. 49 (No. 17) (2010) 8086–8093.
[11] S. Walspurger, L. Boels, P.D. Cobden, G.D. Elzinga, W.G. Haije, R.W. van den Brink, R.Wvaden Brink, The crucial role of the K+ +-aluminium oxide interaction in K+ +-promoted alumina- and hydrotalcite-based materials for CO2 sorption at high temperatures, ChemSusChem 1 (No. 7) (2008) 643–650 Jan..
[12] E.L.G. Oliveira, C.A. Grande, A.E. Rodrigues, CO2 sorption on hydrotalcite and alkali-modified (K and Cs) hydrotalcites at high temperatures, Sep. Purif. Technol. 62 (2008) 137–147.
[13] W. Reichle, S. Kang, D. Everhardt, The nature of the thermal decomposition of a catalytically active anionic clay mineral, J. Catal. 101 (No. 7) (1986) 352–359.
[14] J. Boon, P.D. Cobden, Ha.J. van Dijk, M. van Sint Annaland, High-temperature pressure swing adsorption cycle design for sorption-enhanced water–gas shift, Chem. Eng. Sci. 122 (2015) 219–231 Jan..
[15] J. Boon, P.D. Cobden, Ha.J. van Dijk, C. Hoogland, E.R. van Selow, M. van Sint Annaland, Isotherm model for high-temperature, high-pressure adsorption of and on K-promoted hydrotalcite, Chem. Eng. J. 248 (2014) 406–414 Jul..
[16] J. Boon, V. Spallina, Y. van Delft, M. van Sint Annaland, Comparison of the efficiency of carbon dioxide capture by sorption-enhanced water–gas shift and palladium-based membranes for power and hydrogen production, Int. J. Greenhouse Gas Control 50 (2016) 121–134.
[17] T. Dixon, K. Yamaji, B. Najmi, O. Bolland, S.F. Westman, Simulation of the cyclic operation of a PSA-based SEWGS process for hydrogen production with CO2 capture, Energy Procedia 37 (No. 1876) (2013) 2293–2302.
[18] M. Gazzani, E. Macchi, G. Manzolini, CO2 capture in natural gas combined cycle with SEWGS. part A: thermodynamic performances, Int. J. Greenhouse Gas Control 12 (2013) 493–501.
[19] K. Coenen, F. Gallucci, G. Pio, P. Cobden, E. van Dijk, E. Hensen, M. van Sint Annaland, On the influence of steam on the CO2 chemisorption capacity of a hydrotalcite-based adsorbent for SEWGS applications, Chem. Eng. J. 314 (2017) 554–569.
[20] M. Maroño, Y. Torreiro, L. Gutierrez, Influence of steam partial pressures in the CO2 capture capacity of K-doped hydrotalcite-based sorbents for their application to SEWGS processes, Int. J. Greenhouse Gas Control 14 (2013) 183–192.
[21] A. Zhenissova, F. Micheli, L. Rossi, S. Stendardo, P.U. Foscolo, K. Gallucci, Experimental evaluation of Mg- and Ca-based synthetic sorbents for CO2 capture, Chem. Eng. Res. Des. 92 (No. 4) (2014) 727–740.
[22] S. Walspurger, S. de Munck, P.D. Cobden, W.G. Haije, R.W. van den Brink, O.V. Safonova, Correlation between structural rearrangement of hydrotalcite-type materials and CO2 sorption processes under pre-combustion decarbonisation conditions, Energy Procedia 4 (2011) 1162–1167 Jan..
[23] M. León, E. Díaz, S. Bennici, A. Vega, S. Ordóñez, A. Auroux, Adsorption of CO2 on hydrotalcite-derived mixed oxides: sorption mechanisms and consequences for adsorption irreversibility, Ind. Eng. Chem. Res. 49 (No. 8) (2010) 3663–3671.
[24] S. Walspurger, P.D. Cobden, W.G. Haije, R. Westerwaal, G.D. Elzinga, O.V. Safonova, In situ XRD detection of reversible dawsonite formation on alkali promoted alumina: a cheap sorbent for CO2 capture, Eur. J. Inorg. Chem. 2010 (No. 17) (2010) 2461–2464 Jun..
[25] K. Coenen, F. Gallucci, P. Cobden, E. van Dijk, E. Hensen, M. van S. Annaland, E. van Dijk, E. Hensen, M. van Sint Annaland, Chemisorption working capacity and kinetics of CO2 and H2O of hydrotalcite-based adsorbents for sorption-enhanced water-gas-shift applications, Chem. Eng. J. 293 (2016) 9–23.
[26] F. Prinetto, G. Ghiotti, V.P. Giuria, R. Durand, D. Tichit, Investigation of acid - base properties of catalysts obtained from layered double hydroxides, J. Phys. Chem. B 104 (2000) 11117–11126.
[27] H. Du, C.T. Williams, A.D. Ebner, J.A. Ritter, In situ FTIR spectroscopic analysis of carbonate transformations during adsorption and desorption of CO2 in K-promoted HTlc, Chem. Mater. 22 (No. 11) (2010) 3519–3526.
[28] M.R. Othman, N.M. Rasid, W.J.N. Fernando, Mg-Al hydrotalcite coating on zeolites for improved carbon dioxide adsorption, Chem. Eng. Sci. 61 (No. 5) (2006) 1555–1560.
[29] G. Ramis, G. Busca, V. Lorenzelli, Low-temperature CO2 adsorption on metal oxides: spectroscopic characterization of some weakly adsorbed species, Mater. Chem. Phys. 29 (No. 1–4) (1991) 425–435.
[30] J.C. Lavalley, Infrared studies of the surface acidity of oxides and zeolites using adsorbed probe molecules, Catal. Today 27 (No. 3–4) (1996) 377–401.
[31] G. Busca, V. Lorenzelli, Infrared spectroscopic identification of species arising from reactive adsorption of carbon oxides on metal oxide surfaces, Mater. Chem. 7 (No. 1) (1982) 89–126.
[32] B.H. Stuart, Infrared Spectroscopy: Fundamentals and Applications, John Wiley & Sons, Ltd, Chichester, UK, 2005.
[33] H. Prescott, Z. Li, E. Kemnitz, A. Trunschke, J. Deutsch, H. Lieske, A. Aoroux, Application of calcined Mg–Al hydrotalcites for Michael additions: an investigation of catalytic activity and acid–base properties, J. Catal. 234 (No. 1) (2005) 119–130.
[34] W. Xu, C.T. Johnston, P. Parker, S.F. Agnew, Infrared study of water sorption on Na-, Li-, Ca-, and Mg-exchanged (SWy-1 and SAz-1) montmorillonite, Clays Clay Miner. 48 (No. 1) (2000) 120–131.
[35] J.D. Schuttlefield, D. Cox, V.H. Grassian, An investigation of water uptake on clays minerals using ATR-FTIR spectroscopy coupled with quartz crystal microbalance measurements, J. Geophys. Res. Atmos. 112 (No. 21) (2007) 1–14.
[36] Ja. Lercher, C. Gründling, G. Eder-Mirth, J.C. Lavalley, Infrared studies of the surface acidity of oxides and zeolites using adsorbed probe molecules, Catal. Today 27 (No. 3–4) (1996) 353–376.